Raman spectroscopic study of cation disorder in poly- and single crystals of the nickel aluminate spinel

2007 J. Phys.: Condens. Matter 19 186217

(http://iopscience.iop.org/0953-8984/19/18/186217)

IOP PUBLISHING JOURNAL OF PHYSICS: CONDENSED MATTER

J. Phys.: Condens. Matter **19** (2007) 186217 (10pp) doi:10.1088/0953-8984/19/18/186217

Raman spectroscopic study of cation disorder in poly- and single crystals of the nickel aluminate spinel

M A Laguna-Bercero, M L Sanjuán and R I Merino

Instituto de Ciencia de Materiales de Aragón, CSIC—Universidad de Zaragoza, Pedro Cerbuna 12, 50009 Zaragoza, Spain

E-mail: malaguna@unizar.es

Received 15 January 2007, in final form 14 March 2007
Published 11 April 2007
Online at stacks.iop.org/JPhysCM/19/186217

Abstract

The Raman spectrum of $NiAl_2O_4$ inverse spinel has been studied in quenched polycrystalline pellets produced by solid-state reaction and in single crystals grown by the floating zone method. The lattice parameters and inversion degrees were determined by x-ray diffraction. Polarization measurements in single crystals allow mode symmetry assignment. Then, a correlation is established between the bands observed in polycrystalline samples and those of single crystals. Both kinds of sample present more bands than the five expected ($A_{1g} + E_g + 3T_{2g}$) in a cubic *Fd3m* spinel. This multiplicity is attributed to the almost fully inverted cation distribution in $NiAl_2O_4$, with inversion parameter $x \approx 0.9$. The multiplicity of the high-frequency A_{1g} band, in particular, is attributed to the different possible configurations of Ni^{2+} and Al^{3+} cations occupying the three octahedral sites close to a given oxygen ion. A strong downshift of the E_g mode frequency, as compared to the normal spinel $MgAl_2O_4$, is attributed to the longer bonding distance between oxygen and octahedral cations in inverse II–III spinels. Due to the small range of variation of x upon thermal treatment in $NiAl_2O_4$, no significant differences were found between the spectra of samples quenched at different temperatures, from 800 to 1200 °C.

1. Introduction

Nickel aluminate spinel has been applied in various fields due to its high thermal stability and specific catalytic properties. This material is one of the best supporting catalysts for various metals and oxides [1, 2]. It has also been proposed as a promising candidate anode for aluminium electrolysis [3] and for internal reforming solid oxide fuel cell (IR-SOFC) anodes [4]. Nickel aluminate spinel can be prepared by many methods, such as solid-state reaction [5], microwave-induced sintering [6] or the floating zone technique [7].

The general formula of a II–III spinel is $A^{2+}B_2^{3+}O_4$. In a normal spinel compound, like $MgAl_2O_4$, the divalent and trivalent cations occupy tetrahedral and octahedral sites, respectively. In an inverse spinel the trivalent cations occupy all the tetrahedral sites, while the octahedral sites are filled by all the divalent and half of the trivalent cations. Intermediate situations can arise, and an inversion parameter x is usually defined as the site occupancy factor of trivalent cations on the tetrahedral site.

$NiAl_2O_4$ is a partially inverse spinel with x between 0.8 and 0.9 [8]. The inversion degree of $NiAl_2O_4$ has previously been studied by optical transmission experiments and x-ray diffraction studies as well as its relaxation kinetics after quenching [9, 10]. It is well known that the inversion degree of $NiAl_2O_4$ is a function of temperature [8], being nearly inverse ($x \rightarrow 0.9$) at low temperatures and tending to random distribution ($x = 2/3$) as the temperature increases [11]. A number of previous studies confirm that $NiAl_2O_4$ becomes less inverse when increasing the quenching temperature, up to values of about $x = 0.80$ at 1200 °C [12]. Above 1250 °C the cation redistribution becomes so fast that is not possible to quench properly; below 800 °C the rate of cation diffusion becomes so slow that a complete internal equilibrium is hardly reached [8].

In the present work we have studied the Raman spectrum of the $NiAl_2O_4$ spinel. Apart from its technological interest, we have chosen $NiAl_2O_4$ because there are just a few works about vibrational properties of inverse II–III spinels [13–15]. In such systems, the analysis of the spectrum is complicated by cation disorder between the tetrahedral and octahedral sites.

For this study we have prepared $NiAl_2O_4$ as ceramic pellets and single crystals. The $NiAl_2O_4$ single crystal, although nickel defective, is essential for mode symmetry assignment. Thermal treatments on stoichiometric ceramic samples were performed to change the inversion parameter, whose value was determined by x-ray diffractometry.

2. Experimental procedures

NiO (Aldrich, 99.99%) and Al_2O_3 (Aldrich, 99.99%) powders were milled, calcined and mixed. Ceramic pellets were obtained by uniaxial pressing at 50 MPa followed by sintering at 1500 °C during 48 h. The final density of the samples was about 55%. Precursor rods for the single crystals, 2 mm in diameter and 50 to 100 mm in length, were prepared from a mixture of the oxide powders via pressureless sintering during 48 h at 1500 °C. Nickel aluminate single crystals were grown using a floating zone (FZ) method as described elsewhere [16]. A feed rod was flexibly attached to the upper shaft, while a polycrystalline support of the same composition was rigidly fixed to the lower shaft. The shafts were counter-rotated at 17 rpm and, after forming a liquid zone, the seed and feed rods were joined. Then the mirrors were translated vertically at a rate of 10 mm h^{-1}. The whole process was performed in air. The crystallographic orientation of the single crystal was determined with axial photographs using the back-reflection Laue method [17].

Thermal treatments in ceramic samples were performed in a furnace followed by quenching in water. The annealing times were selected according to the previous study of Becker [18]. He calculated relaxation times of the cationic distribution in nickel aluminate as a function of temperature. X-ray diffraction experiments (XRD) were carried out using a Rigaku rotating anode x-ray generator RU-300 and using silicon as a standard. Scanning electron microscope (SEM) electron probe microanalyses (EPMA) were carried out with a JEOL 6400 microscope equipped with a Link Analytical eXL analyser using standard compounds of Cu, Ni and α-Al_2O_3. Raman measurements were performed in the backscattering configuration at room temperature (RT) in a DILOR XY spectrometer with a liquid-nitrogen-cooled charge-coupled device (CCD) detector and excitation through the microscope, using the 496.5 and 514.5 nm lines of an Ar^+ laser. The Si mode at 520 cm^{-1} was used for frequency calibration.

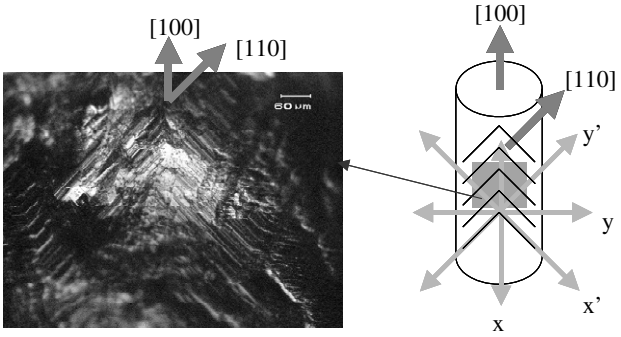

Figure 1. (a) Optical photograph of the surface of the FZ grown cylinder. (b) Schema showing the x, x', y and y' directions used to register the polarized Raman spectra.

3. Experimental results

3.1. Single-crystal characterization

The chemical composition of the nickel aluminate single crystal was determined by energy dispersive spectroscopy (EDS) microanalysis in the SEM. The results obtained were (in at. per formula) 0.709 ± 0.003 Ni and 2.194 ± 0.011 Al. These results show that this single crystal is nickel defective, due to continuous NiO evaporation during growth, as was also observed by Subramanian *et al* [7]. In fact, according to the NiO–Al_2O_3 phase diagram [19], the resulting composition is close to the stability limit of the spinel phase in Al_2O_3-rich systems. The spinel structure can accept up to a 15 mol% excess of Al_2O_3 at temperatures about 2000 °C.

The single crystal obtained by the floating zone method was analysed by the back-reflection Laue method. Axial photographs were obtained along the growth direction, confirming the single-crystallinity of the sample. From those photographs, the crystal was oriented determining that the growth direction coincides with one of the cubic ⟨100⟩ axes. Square-like facets are observed in the surface of the crystal, with edges parallel to ⟨110⟩ directions (x'/y' axes) (figure 1). This crystal, although nickel defective, presents cubic symmetry; its powder XRD can be fitted with the *Fd3m* (O_h^7) space group of cubic spinels with a lattice parameter $a = 8.0119 \pm 1 \times 10^{-3}$ Å, quite small compared with that of the stoichiometric nickel aluminate spinel (8.0451 Å) [8]. This difference is a consequence of the nickel deficiency of the single crystal. Due to this non-stoichiometry, we shall not use the single crystal for cation distribution studies, since the inversion parameter is probably altered by the presence of aluminium excess and cation vacancies. The single crystal has been used for symmetry assignment of Raman modes. To analyse the Raman spectra of stoichiometric samples and to explore the dependence of Raman modes on cation distribution, we have used stoichiometric ceramic samples.

3.2. Characterization of quenched ceramic samples by x-ray diffractometry

The chemical composition of the as-grown ceramic samples was determined by EDS microanalysis in the SEM. The results obtained were (in at. per formula) 1.048 ± 0.004 Ni and 1.928 ± 0.010 Al.

To guarantee that the samples where homogeneously equilibrated at the annealing temperature and properly quenched, the lattice and inversion parameters were determined and compared with the literature values. The samples also present a face-centred cubic structure

Table 1. Lattice and inversion parameters of samples quenched between 800 and 1200 °C obtained from their XRD patterns.

Quenching temperature (°C)	Lattice parameter (Å)	Inversion parameter x
800	$8.0459 \pm 9 \times 10^{-4}$	0.873
900	$8.0466 \pm 9 \times 10^{-4}$	0.860
1100	$8.0496 \pm 9 \times 10^{-4}$	0.818
1200	$8.0530 \pm 7 \times 10^{-4}$	0.803

(*Fd3m*). The lattice parameters of samples quenched between 800 and 1200 °C are given in table 1. The lattice parameter increases by almost 0.1% with quenching temperature from 800 to 1200 °C.

To determine the inversion degree we have simulated the x-ray diffractogram as a function of the cationic distribution among tetrahedral and octahedral sites (with fixed $u = 0.256$) [12], and looked at the relative intensity between the [400] and the [311] peaks, the most sensitive to the inversion and the most intense, respectively. The results of the inversion degree parameters obtained for samples quenched between 800 and 1200 °C are also given in table 1. Lattice parameters and inversion degrees are in good agreement with the results obtained by Roelofsen *et al* [12] and O'Neill *et al* [8].

3.3. Raman dispersion

The unit cell of a cubic spinel with space group *Fd3m* presents 42 degrees of freedom, 39 of them corresponding to optical modes and the three others to acoustic modes. At zone centre, optical modes belong to the following symmetries [20]:

$$\Gamma = A_{1g} + E_g + 3T_{2g} + 4T_{1u} + T_{1g} + 2A_{2u} + 2E_u + 2T_{2u}$$

from which A_{1g}, E_g and T_{2g} modes are Raman active and T_{1u} are infrared active. Raman selection rules are determined by the polarization tensors which, for O_h symmetry and the reference system formed by the $\langle 100 \rangle$ directions, are:

$$A_{1g} = \begin{pmatrix} a & 0 & 0 \\ 0 & a & 0 \\ 0 & 0 & a \end{pmatrix} \qquad E_g = \begin{pmatrix} b & 0 & 0 \\ 0 & -b & 0 \\ 0 & 0 & 0 \end{pmatrix}, \frac{1}{\sqrt{3}} \begin{pmatrix} b & 0 & 0 \\ 0 & b & 0 \\ 0 & 0 & -2b \end{pmatrix}$$

$$T_{2g} = \begin{pmatrix} 0 & d & 0 \\ d & 0 & 0 \\ 0 & 0 & 0 \end{pmatrix}, \begin{pmatrix} 0 & 0 & d \\ 0 & 0 & 0 \\ d & 0 & 0 \end{pmatrix}, \begin{pmatrix} 0 & 0 & 0 \\ 0 & 0 & d \\ 0 & d & 0 \end{pmatrix}.$$

Along these axes, both A_{1g} and E_g modes appear with the same selection rules. To separate them, it is necessary to measure in other configurations. For that reason, a new reference system is taken by a 45° rotation around one of the three quaternary axes (the z axis for convenience, which is assumed to be the direction of light propagation). Thus, the new reference system is formed by the [110], [1$\bar{1}$0] and [001] directions (x', y', z); in these axes the Raman tensors are written as

$$A_{1g} = \begin{pmatrix} a & 0 & 0 \\ 0 & a & 0 \\ 0 & 0 & a \end{pmatrix} \qquad E_g = \begin{pmatrix} 0 & b & 0 \\ b & 0 & 0 \\ 0 & 0 & 0 \end{pmatrix}, \frac{1}{\sqrt{3}} \begin{pmatrix} b & 0 & 0 \\ 0 & b & 0 \\ 0 & 0 & -2b \end{pmatrix}$$

$$T_{2g} = \begin{pmatrix} d & 0 & 0 \\ 0 & -d & 0 \\ 0 & 0 & 0 \end{pmatrix}, \frac{1}{2} \begin{pmatrix} 0 & 0 & -d \\ 0 & 0 & d \\ -d & d & 0 \end{pmatrix}, \frac{1}{2} \begin{pmatrix} 0 & 0 & d \\ 0 & 0 & d \\ d & d & 0 \end{pmatrix}.$$

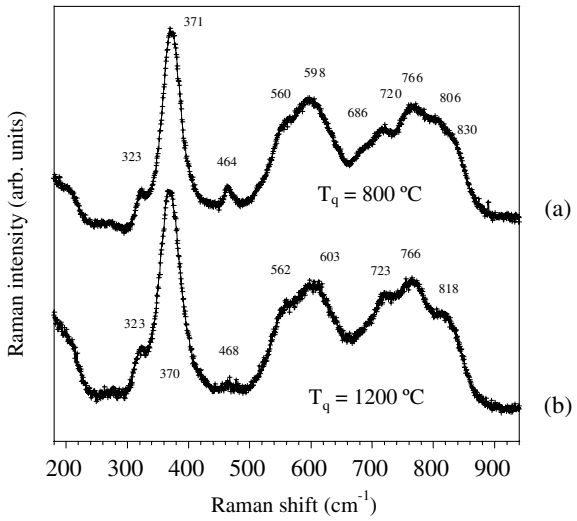

Figure 2. RT Raman spectra of polycrystalline $NiAl_2O_4$ samples, equilibrated at 800 °C (a) and 1200 °C (b), and then quenched in water.

Figure 2 shows the Raman spectrum of polycrystalline $NiAl_2O_4$. Spectra (a) and (b) belong to samples equilibrated at 800 and 1200°C, respectively, and then quenched in water. Both spectra are very similar and present three groups of lines: an intense line at $\nu \approx 370$ cm^{-1}, accompanied by a weak side-band at $\nu \approx 323$ cm^{-1}, a group of broad bands of medium intensity between 500 and 650 cm^{-1}, and a large structured band extending from 650 to 850 cm^{-1}. The similarity of the lattice parameter of $NiAl_2O_4$ with those of other aluminate spinels makes it tempting, as a first approximation, to assign the bands of $NiAl_2O_4$ by comparison with related compounds, for instance with $MgAl_2O_4$, the prototype spinel oxide [21–24]. As previously explained, only five Raman active modes are expected in a normal cubic spinel: $A_{1g} + E_g + 3T_{2g}$. On average, i.e. neglecting local non-periodicity, the same count is valid for inverse spinels, provided that their structure can still be described as cubic with *Fd3m* space group. Thus, the intense band at 370 cm^{-1} and its low-frequency shoulder would be attributed to the E_g and low-frequency T_{2g} modes, respectively (at 410 and 311 cm^{-1} in $MgAl_2O_4$); the bands in the intermediate-frequency region would be the other two T_{2g} (492 and 671 cm^{-1} in $MgAl_2O_4$), and the whole of the high-frequency band might be attributed to different forms of the A_{1g} mode expected in a normal spinel (770 cm^{-1} in $MgAl_2O_4$) [21, 22, 24].

However, the spectra of $NiAl_2O_4$ present some anomalies, such as the multiplicity of the high-frequency band and the frequency shifts compared with those of the corresponding modes in $MgAl_2O_4$, that suggest that this assignment may be too simple. These anomalies are attributed to the inverse character of $NiAl_2O_4$, which is, to our knowledge, the only aluminate spinel with almost fully inverted cation distribution ($ZnAl_2O_4$ is a normal spinel [25], $CuAl_2O_4$ has $x \approx 0.3$ [25] and $x \approx 0.2$ for $CoAl_2O_4$ [26]).

Since light becomes depolarized in polycrystalline samples, measurements in single crystals are required to reach a reliable mode assignment. Single-crystal measurements were performed in backscattering configuration onto two different surfaces: the transverse section of the FZ rod, identified as a (100) plane, and a side flat surface with clear facets with edges at 90° from each other, also identified as a (100) plane (see figure 1). Since the edges of the side

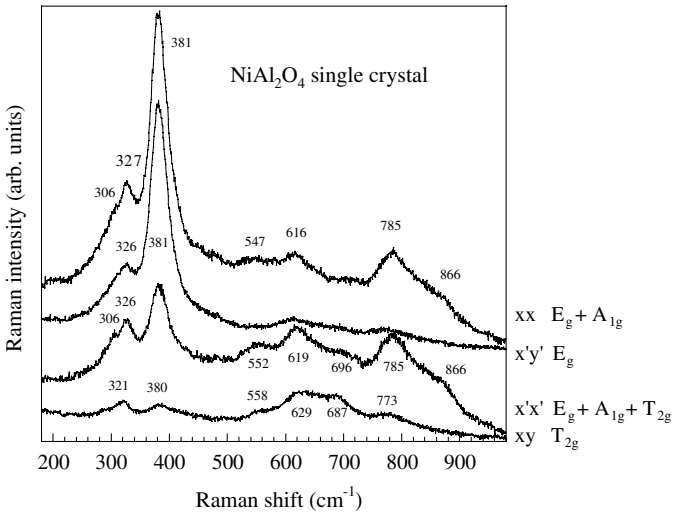

Figure 3. Raman spectra recorded onto a (001) side face of the $NiAl_2O_4$ single crystal in backscattering geometry. The $\alpha\beta$ labelling stands for the incident and scattered electric field polarization, assuming that light propagates along the $z \parallel [001]$ crystal axis. For the definition of $\{x, y\}$ and $\{x', y'\}$ axes, see the text.

face could be easily identified as $\langle 110 \rangle$ directions, sample orientation was more precise in this face. Figure 3 shows the spectra recorded onto the side face of the $NiAl_2O_4$ single crystal in backscattering geometry. The $\alpha\beta$ labelling of the spectra stands for the incident and scattered electric field polarization, assuming for convenience that incident and scattered light propagates along the $z \parallel [001]$ crystal axis.

With the use of Raman tensors appropriate to cubic symmetry, it is straightforward to see that xy and $x'y'$ configurations yield T_{2g} and E_g modes, respectively, while A_{1g} modes can be found by exclusion or by combining spectra to suppress the contribution of other symmetries. Following this procedure, we arrive at the symmetry assignment presented in table 2. We note that, in general, good fulfilment of the selection rules is found, in the sense that each band can be given a definite A_{1g}, E_g or T_{2g} symmetry, although for all symmetries the number of observed bands is higher than expected for a cubic spinel. Such multiplicity is typical of inverse spinels such as $NiAl_2O_4$, with tetrahedral sites almost fully occupied by Al^{3+} ions and random occupation of the octahedral sites by Al^{3+} and Ni^{2+} ions. A closer look at the spectra of figure 3 and the mode symmetries given in table 2 shows that two kinds of extra modes appear: (i) a multiplication of each spinel mode into two or more bands at close frequencies; (ii) extra bands in regions where no mode is expected for a II–III spinel oxide.

4. Discussion

It is tempting to assign the multiplicity of each spinel mode as arising from the coexistence of two types of domains, with either normal or inverse types of cation distribution. This is the interpretation usually proposed to explain the appearance of some weak extra lines in synthetic $MgAl_2O_4$ or in spinels subjected to thermal treatments favouring cation disorder [23, 24]. Though this explanation may be valid for systems with very low inversion parameter, we think that it does not fully account for the duplication of modes in $NiAl_2O_4$. If the model were valid, one would expect relative intensities in each pair of modes to be roughly proportional to the fraction of inverse and normal regions [27] x and $1 - x$, respectively, which is about 85% and

Table 2. Raman shifts (cm^{-1}) and mode symmetry of $NiAl_2O_4$ spinel. The mode assignment has been made on single-crystal samples. A tentative correlation between ceramic and single-crystal modes is proposed (see the text). A question mark indicates a possible mode at a close frequency that may be masked under the most intense one. w: weak; sh: shoulder; m: medium; s: strong.

Raman shifts, single crystal	Mode symmetry, single crystal	Raman shifts, ceramic samples	Mode assignment, ceramic samples
304 (sh), 330 (w)	A_{1g}	686	A_{1g} (+ T_{2g}?)
548 (w), 618 (w)		720	A_{1g} (+ T_{2g}?)
785 (m), 866 (m)		766	A_{1g}
		800–830	A_{1g}
326 (m), 381 (s)	E_g	370	E_g
		468	?
321 (w), 380 (leak)	T_{2g}	323	T_{2g} (+ E_g?) (+ A_{1g}?)
558 (sh), 629 (m)		564	T_{2g} (+ A_{1g}?)
687 (m), 773 (w)		600	T_{2g} (+ A_{1g}?)

15% in our $NiAl_2O_4$ samples. This proportionality may be fulfilled by the E_g modes at 326 and 370 cm^{-1}, but not by the triplet and singlet bands. Moreover, as we shall see later, the E_g mode of normal domains is expected at higher frequency than that of inverse domains, thus it cannot be assigned to the 326 cm^{-1} feature. Without excluding that contribution, it seems that there is another mechanism activating extra modes.

Different mechanisms have been proposed to explain the appearance of extra lines in inverse spinels, besides the attribution to normal or inverted-type domains. Among them, those based on long-range symmetry descent by cation ordering or shift [13, 14] can be discarded in our case, since XRD can be fitted to the cubic *Fd3m* space group without any evidence of such lower symmetry. However, local distortions, up to an extent of several unit cells, would not be detected by XRD and are likely to occur due to the structural disorder inherent to inverse spinels. Local distortions may relax the usual selection rules of cubic spinels, activate Raman forbidden modes and, finally, split doubly or triply degenerate modes into singlet or doublet modes.

Another source of structural disorder possibly yielding extra modes in the spectra of our $NiAl_2O_4$ single crystals is their defective stoichiometry, due to Ni evaporation during the FZ growing process. According to the microanalysis results, the cation composition of our single crystals is close to $Ni_{0.7}Al_{2.2}$, which means that 0.1 cation sites per formula are left vacant to compensate the excess charge of Al^{3+} replacing the lost Ni. Due to the smaller radius of Al^{3+} compared to Ni^{2+}, Ni deficiency results in a smaller lattice parameter of the $NiAl_2O_4$ single crystal ($a = 8.01$ Å instead of 8.05 Å for stoichiometric $NiAl_2O_4$) and, as a consequence, higher vibrational frequencies for the single crystal than for polycrystalline samples, as observed.

Lattice contraction is not the only effect of Ni evaporation: the altered proportion of Ni/Al ions, as well as the presence of some cation vacancies, may yield extra local distortions and modes, so that a full correlation cannot be established between the spectra of single crystals and those of ceramic samples. Some weak features appearing in the single crystal, such as the extra A_{1g} modes at $\nu \approx 300$ cm^{-1} and in the 500–600 cm^{-1} region, do not have a clear correspondence in polycrystalline samples, a fact that may just be a consequence of band overlap between modes of close frequencies in the polycrystalline samples, or due to the extra defectiveness of the single-crystal sample. The mode assignment for the ceramic samples given in table 2 is only tentative and based on comparison with single-crystal results.

We now focus on the origin of the multiple high-frequency A_{1g} bands. Since group theory says that only one A_{1g} mode is expected, its normal mode displacements are coincident with the symmetry coordinate [28]. In the A_{1g} mode, oxygen atoms vibrate along the direction joining an oxygen ion to the tetrahedral cation M_t, a fact that has led many researchers to attribute the A_{1g} mode to the breathing motion of the M_t–O_4 tetrahedron. This picture would be valid if M_t–O_4 tetrahedra were isolated from the rest of the lattice, or if at least the M_t–O bonds were much stronger than that between the octahedral cation M_o and oxygen, a condition that is not fulfilled in the spinel structure. In contrast, the A_{1g} mode involves, together with the stretching of the M_t–O bond, the deformation of three M_o–O bonds. In fact, the analytical expression given by Gupta *et al* for $\nu_1 = \nu(A_{1g})$ in terms of short-range force constants [29] implies that the M_o–O stretching force constant is as determinant as the M_t–O one for the value of ν_1. A strong contribution of next-nearest-neighbour interactions between atoms of the same type is also expected. In this line, Preudhomme and Tarte [15] proposed that ν_1 is mainly determined by the nature of the highest-valence cation and its bond distance to oxygen, irrespective of whether it is at the tetrahedral or octahedral site. In fact, a look at the ν_1 values of II–III spinel oxides, either normal or inverse, shows that data are grouped according to the trivalent cation: aluminates have ν_1 between 750 and 800 cm^{-1}, while ν_1 lies between 650 and 700 cm^{-1} for ferrites and chromites.

Another argument against the attribution of ν_1 as being exclusively the tetrahedron breathing mode is that, $NiAl_2O_4$ being an almost completely inverted spinel, a single breathing mode corresponding to the Al–O bond stretching would be expected, while there are at least three components in the high-frequency band of A_{1g} symmetry.

In the assumption that bonding with the octahedral cations is as relevant as with the tetrahedral cation for the A_{1g} mode frequency, the appearance of several A_{1g} subbands can be explained as arising from the different possible configurations of Al and Ni cations occupying the three octahedral sites nearest to each oxygen ion. There are four such combinations: 3Ni, 2Ni + 1Al, 1Ni + 2Al, and 3Al. Taking into account that, for a stoichiometric spinel with inversion factor $x \approx 0.85$, the occupancy of the octahedral site is $Al_{1.15}Ni_{0.85}$, we can apply the binomial formula for the statistical probability of each configuration to find $P(3Ni) = 0.077$; $P(2Ni + 1Al) = 0.312$; $P(1Ni + 2Al) = 0.422$; $P(3Al) = 0.190$.

In calculating these figures we have assumed that Al^{3+} occupies all tetrahedral sites. Another set of figures would be given by the preceding figures multiplied by 0.15/0.85, to account for *normal* domains with Ni^{2+} in the T site. These numbers are much smaller than those for the *inverse* domains and will be neglected for simplicity. One thus sees that two of the configurations (namely those having a mixture of Ni^{2+} and Al^{3+} ions) will occur with probability above 30%, while those with three equal cations have probabilities between ≈8 and 20%. As a first approximation, and regarding that these numbers represent a purely statistical calculation with no energetic balance considered, this model may explain the appearance of extra A_{1g} bands. Due to the higher charge of Al^{3+} compared to Ni^{2+}, the frequency corresponding to each configuration is expected to increase with increasing number of Al^{3+} neighbours in the octahedral sites, $\nu(3Ni) \lesssim \nu(2Ni + 1Al) \lesssim \nu(1Ni + 2Al) \lesssim \nu(3Al)$. Unfortunately, due to disorder-induced broadening, the accuracy of our Raman spectra is not enough to correlate the relative intensities of the bands with the expected statistical abundances in going from $x = 0.803$ (1200 °C quench temperature) to 0.873 (800 °C).

With regard to the E_g mode, it is striking that it does not present the same split aspect as the A_{1g} band. The appearance of a second E_g band as a shoulder of the main band, clearly visible in the $x'y'$ spectra of the single crystal, is not so evident in the ceramic samples, where the low-frequency sideband is weaker and narrower, and might arise just from the expected

low-frequency T_{2g} mode. We remember that the single crystal is defective and might show additional spectral features.

Another remarkable aspect of the E_g band is its low frequency, compared to that of $MgAl_2O_4$, especially if we consider that the $NiAl_2O_4$ lattice ($a = 8.05$ Å) is more compressed than that of $MgAl_2O_4$ ($a = 8.08$ Å). At this point, it is worth looking in more detail at the structural differences between normal and inverse spinels [30]. In normal spinels, Coulombic forces push oxygen atoms toward the octahedral sites, occupied by trivalent cations, resulting in an oxygen coordinate u of about 0.26 and almost equal distances from oxygen to tetrahedral (d_t) and octahedral (d_o) cations: $d_t = 1.922$, $d_o = 1.926$ Å in $MgAl_2O_4$ [31]. In inverse spinels, oxygen ions shift toward tetrahedral Al^{3+} cations, resulting in $u \approx 0.25$ and $d_t \ll d_o$ ($d_t = 1.81$ Å and $d_o = 1.97$ Å in $NiAl_2O_4$) [32]. Now, a compilation of data of II–III spinel oxides shows that $\nu(E_g)$ is closely related to the oxygen-octahedral cation bond distance. The analytical expression given by Gupta *et al* [29] also implies an almost negligible dependence of $\nu(E_g)$ on the oxygen bonding to the tetrahedral cation. Thus, the decrease in $\nu(E_g)$ observed in $NiAl_2O_4$ is attributed to the longer O–M_o bond, which, in turn, is due to the inverse character of $NiAl_2O_4$. In support of this interpretation, we note that, in the high-temperature Raman spectra of $MgAl_2O_4$ reported previously [21], a shoulder appears *on the low-frequency side* of the normal E_g mode on increasing temperature, a fact that is attributed to the redistribution of Al^{3+} cations on the tetrahedral site to yield a partially inverse spinel.

5. Conclusions

We have studied for the first time the vibrational properties of $NiAl_2O_4$, which is the only known aluminate spinel with almost fully inverted cation distribution. Raman spectra are recorded on quenched polycrystalline ceramic samples and in single crystals grown by the floating zone method. In the latter, Ni deficiency results in a smaller lattice parameter. As a consequence, higher vibrational frequencies are observed for the single crystal than for polycrystalline samples.

Polarized Raman studies on oriented single crystals have allowed us to determine the symmetry of the vibrational modes. Up to six A_{1g}, six T_{2g} and two E_g bands are detected in the single crystal. Extra lines are also observed in polycrystalline samples, as compared with a normal cubic spinel. The multiplicity of the bands is attributed to the disordered character of cation distribution in $NiAl_2O_4$. In particular, the appearance of several high-frequency A_{1g} subbands is explained with a simple model that considers the different possible configurations of Al^{3+} and Ni^{2+} cations occupying the three octahedral sites nearest to each oxygen ion. The anomalously low frequency of the E_g band (370 cm^{-1}) is attributed to the longer oxygen–octahedral cation bond due to the inverse character of $NiAl_2O_4$.

Though our results are interpreted on the basis of the inverse character of $NiAl_2O_4$, the range of inversion parameter x achievable experimentally is too narrow, so such small variations do not have any significant effect on the Raman spectrum.

Acknowledgments

The authors would like to thank Dr A Larrea for his assistance with the SEM experiments and J Blasco for his help in growing the $NiAl_2O_4$ single crystal. Financial support from projects MAT2003-1182, MAT2004-03070-C05-03 and MAT2006-13005-C03-01 is also acknowledged.

References

[1] Rodríguez J C, Romeo E, Fierro J L G, Santamaría J and Monzón A 1997 *Catal. Today* **37** 255–65
[2] Huang Y J, Schwarz J A, Dile J R and Baltrus J A 1988 *Appl. Catal.* **36** 163–75
[3] Han Y S, Li J B, Ning X S and Chi B 2005 *J. Am. Ceram. Soc.* **88** 3455–7
[4] Kou L and Selman J R 2000 *J. Appl. Electrochem.* **30** 1433–7
[5] Han S, Li J B, Ning X S and Chi B 2004 *J. Am. Ceram. Soc.* **87** 1347–9
[6] Peelamedu R D, Roy R and Agrawal D K 2002 *Mater. Lett.* **55** 234–40
[7] Subramanian R, Higuchi M and Dieckman R 1994 *J. Cryst. Growth* **143** 311–6
[8] O'Neill H St C, Dollase W A and Ross C R 1991 *Phys. Chem. Mineral.* **18** 302–19
[9] Becker K D and Rau F 1987 *Ber. Bunsenges. Phys. Chem.* **91** 1279–82
[10] Röttger R, Schmalzried H and Günter M 1997 *Ber. Bunsenges. Phys. Chem.* **101** 1083–9
[11] Mocala K and Navrotsky A 1989 *J. Am. Ceram. Soc.* **72** 826–32
[12] Roelofsen J N, Peterson R C and Raudsepp M 1992 *Am. Mineral.* **77** 522–8
[13] Malézieux J-M and Piriou B 1988 *Bull. Minéral.* **111** 649–69
[14] Graves P R, Johnston C and Campaniello J J 1988 *Mater. Res. Bull.* **23** 1651–60
[15] Preudhomme J and Tarte P 1971 *Spectrochim. Acta* A **27** 961
Preudhomme J and Tarte P 1972 *Spectrochim. Acta* A **28** 69
[16] Herrero-Martín J, García J, Subías G, Blasco J and Sánchez M C 2004 *Phys. Rev.* B **70** 024408
[17] Azároff L V 1968 *Elements of X-Ray Crystallography* (New York: McGraw-Hill)
[18] Becker K D 1997 *Ber. Bunsenges. Phys. Chem.* **101** 1248–57
[19] Phillips B, Hutta J J and Warshaw I 1963 *J. Am. Ceram. Soc.* **46** 579–83
[20] White W B and de Angelis B A 1967 *Specrochim. Acta* A **23** 985–95
[21] O' Horo A, Frisillo L and White W B 1973 *J. Phys. Chem. Solids* **34** 23
[22] Fraas L M, Moore J E and Salzberg J B 1973 *J. Chem. Phys.* **58** 3585
[23] Cynn H, Sharma S K, Cooney T F and Nicol M 1992 *Phys. Rev.* B **45** 500–2
[24] Chopelas A and Hofmeister A M 1991 *Phys. Chem. Mineral.* **18** 279
[25] Cooley R F and Reed S 1972 *J. Am. Ceram. Soc.* **55** 395
[26] Furuhashi H, Inagaki M and Naka S 1973 *J. Inorg. Nucl. Chem.* **35** 3009
[27] Ursaki V V, Manjón F J, Tiginyanu I M and Tezlevan V E 2002 *J. Phys.: Condens. Matter* **14** 6801
[28] Lutz H D 1969 *Z. Naturf.* a **24** 1417
[29] Gupta H C, Parashar A, Gupta V B and Tripathi B B 1990 *Phys. Status Solidi* b **160** K19
[30] Sickafus K E, Wills J M and Grimes N W 1999 *J. Am. Ceram. Soc.* **82** 3279
[31] Yamanaka T and Takeuchi Y 1983 *Z. Kristallogr.* **165** 65
[32] Otero Areán C and Díez Viñuela J S 1985 *J. Solid State Chem.* **60** 1